Unsupervised Segmentation of Retinal Blood Vessels Using the Human Visual System Line Detection Model

Mohsen Zardadi*
Department of Electrical and Computer Engineering, Birjand University, Birjand, Iran
zardadi@birjand.ac.ir
Nasser Mehrshad
Department of Electrical and Computer Engineering, Birjand University, Birjand, Iran
nmehrshad@birjand.ac.ir
Seyyed Mohammad Razavi
Department of Electrical and Computer Engineering, Birjand University, Birjand, Iran
smrazvi@birjand.ac.ir

Received: 10/Sep/2015 Revised: 30/Apr/2016 Accepted: 16/May/2016

Abstract

Retinal image assessment has been employed by the medical community for diagnosing vascular and non-vascular pathology. Computer based analysis of blood vessels in retinal images will help ophthalmologists monitor larger populations for vessel abnormalities. Automatic segmentation of blood vessels from retinal images is the initial step of the computer based assessment for blood vessel anomalies. In this paper, a fast unsupervised method for automatic detection of blood vessels in retinal images is presented. In order to eliminate optic disc and background noise in the fundus images, a simple preprocessing technique is introduced. First, a newly devised method, based on a simple cell model of the human visual system (HVS) enhances the blood vessels in various directions. Then, an activity function is presented on simple cell responses. Next, an adaptive threshold is used as an unsupervised classifier and classifies each pixel as a vessel pixel or a non-vessel pixel to obtain a vessel binary image. Lastly, morphological post-processing is applied to eliminate exudates which are detected as blood vessels. The method was tested on two publicly available databases, DRIVE and STARE, which are frequently used for this purpose. The results demonstrate that the performance of the proposed algorithm is comparable with state-of-the-art techniques.

Keywords: Retinal Vessel Segmentation; Simple cell Model; DRIVE Database; STARE Database.

1. Introduction

Retinal blood vessel segmentation provides information for diagnosis, treatment, and evaluation of various cardiovascular and ophthalmologic diseases such as hypertensions, diabetes and arteriosclerosis [1]. Various features of retinal blood vessels such as length, width, and tortuosity guide ophthalmologists to diagnose and/or monitor pathologies of different eye anomalies [2-4]. Automatic segmentation of retinal blood vessels is the first step in the development of a computer-assisted diagnostic system. A large number of methods and algorithms that have been published are related to retinal blood vessel segmentation [5]. Each of these methods have their own merits and shortcomings. The algorithms in this field can be classified into techniques based on match filtering, pattern recognition, morphological processing, multiscale analysis and vessel tracking.

As with the processing of most medical images, the signal noise, drift in image intensity, and lack of image contrast cause significant challenges in the extraction of blood vessels. The vessels can be expected to be connected and form a binary treelike structure. However, the shape, size, and local grey level of blood vessels can vary and background features may have similar attributes to vessels.

The vessel intensity profiles approximate to a Gaussian shape, or a mixture of Gaussians. Therefore, Gabor filters, which are a multiplication of Gaussian and cosine functions, may be a good approximation of the vessel intensity profiles. Gabor filters are also utilized to model simple cells in the primary visual cortex. The simple cells in the human visual system respond vigorously to an edge or a line of a given orientation and position. It can be expected that a computational model of a simple cell by a Gabor filter may extract blood vessels effectively.

In this paper, we offer an unsupervised approach for retinal blood vessel segmentation in fundus images. Our method was inspired by operations of the human visual system in perception of edges and lines at different directions. This paper is organized as follows: a review of other published vessel segmentation solutions in section two, a presentation of the proposed method in section three, results and comparisons with other existing methods in section four, and finally, the main conclusions of this work in section five.

2. Related Work

Retinal blood vessel segmentation methods can be divided into two broad categories: unsupervised and

* Corresponding Author

supervised methods. Due to the fast algorithms of unsupervised methods, they are generally preferred over supervised methods for medical decision support systems and real time applications. As the proposed method is also an unsupervised method, it will be more focused on in the review section of this paper.

2.1 Unsupervised Methods

Unsupervised methods perform vessel segmentation without any prior labeling information to decide whether a pixel belongs to a vessel, or not. A match filtering technique is one of the common unsupervised approaches in retinal vessel segmentation [6]. Matched filtering convolves the image with multiple matched filters for detection of blood vessels. The matched filter was first introduced by Chaudhuri et al. [7]; they proposed a two-dimensional linear kernel with a Gaussian profile to detect the blood vessels. The kernel is rotated in 12 directions and the maximum response is selected for each pixel. This method was improved by Hoover et al. [7] who combined local and region-based properties of the vessels. They employed a thresholding technique with iterative probing for each pixel. Gang et al. [8] also extended Chaudhuri et al.'s method by an amplitude-modified second order Gaussian filter. Gang et al. optimized the matched Gaussian filter by the vessel width. To summarize, all of these matched filtering methods suffer from low signal-to-noise ratio (SNR).

There are some unsupervised segmentation methods which improved accuracy and/or speed of the segmentation. Cinsdikici and Aydin in [9] present a combination of ant colony optimization algorithm and a hybrid model of the matched filter. They employ some preprocessing techniques and combine matched filter results with an ant colony algorithm to extract blood vessels. High computational cost and set parameters are the main drawbacks of this approach; however Cinsdikici and Aydin increased the accuracy of match filters.

In order to address high computational costs, Amin and Yan proposed a high speed vessels detection algorithm which extracted blood vessels in 10 seconds for each retinal image [10]. They used a phase congruency to enhance the vessel intensity in the algorithm. The phase congruency of an image is computed by a Log-Gabor wavelet. Afterwards, blood vessels are segmented by using a threshold probing technique on phase congruency response images. In the Amin and Yan method, several phase congruency images should be obtained from a single retinal image for different parameters and the best one is determined based on the ROC curve. The phase congruency image that produces the highest area under the ROC curve is considered an optimum image; and related parameters are recorded. As a result of high computational costs, their method suffers from a complex parameter adjustment procedure.

Zana and Klein [11] presented a different approach to extract the vessels. They used mathematical morphology and curvature evaluation in a noisy environment. Their method is based on four steps: noise reduction, linear pattern with Gaussian-like profile improvement, cross-curvature evaluation and linear filtering. Like other morphological processes, Zana and Klein's method depends heavily on the length of linear structure elements, and causes difficulties with highly tortuous vessels.

Fraz et al. [12] combine vessel centerlines with bit plane slicing to identify the vessel patterns in the retina. Fraz et al. used an orientation map to segment blood vessels. The orientation map of vessels is generated by using a multidirectional top-hat operator with a linear oriented structuring element which emphasizes the vessels in the particular direction. Then, significant information is obtained from the greyscale image using bit plane slicing. Finally, the vessels map is acquired by a combination of the vessel centerlines and the orientation maps. In this method, the vessel centerlines, vessel shape, and orientation maps play crucial roles in the segmentation of the vascular tree. Therefore, because of the prominent light reflection of some vessels like arterioles, and a mismatch between the highest local intensity across the blood vessels and the vessel center, this approach is less suited for all blood vessels in the retinal images. Mendonca et al. [13] also propose a vessel centerline detection in combination with multiscale morphological reconstruction. The vessel centerlines are generated by applying Difference of Offset Gaussian (DoOG) filter. Vessel highlighting is acquired by a modified top hat operator with variable size circular structuring elements. They employ multiscale morphological reconstruction to obtain binary image.

Lam and Yan, on the other hand, propose a vessel segmentation algorithm based on the divergence of vector fields [14]. They locate vessel-like objects by using Laplacian operator and pruning noisy objects based on the centerlines. Consequently, the vessel-like patterns which are far away from the centerlines are removed. Although Lam and Yan's method is almost robust, it is a time-consuming approach. It requires around 25 minutes to produce the vessels for a single retinal image [14]. Recently, Lam et al. have presented a vessel profile model to detect blood vessels [15]. This algorithm is based on regularization-based multi-concavity modeling. A differentiable concavity measure on perceptive space is designed to extract blood vessels in retinal images with bright lesions. A line-shape concavity measure is also presented to distinguish dark lesions from the vessels. The vessels are obtained by a lifting technique. A main disadvantage of Lam et al.'s method is high computational cost. It takes, on average, 13 minutes to extract blood vessels.

Al-Diri et al., alternatively, present an active contour model for segmenting retinal vessels [16]. They detect blood vessels by growing a 'Ribbon of Twins' active contour model which employs two pairs of contours to capture each vessel edge. Initially, a tramline filter is used to locate an initial set of potential vessel segment centerline pixels. Then, the segment growing algorithm converts the tramline image into a set of segments.

Finally, a junction resolution method extends the discrete segments and resolves various crossings and junctions. Al-Diri et al. gained good results, but the method suffers from high computational complexity.

2.2 Supervised Methods

Due to the limited success of unsupervised methods in achieving an acceptable output, some researchers have focused on development of supervised algorithms [17-22]. In supervised methods, observer data (gold standard) is firstly used for the classification of vessels based on given features. Then, a feature vector is required for each pixel. Lastly, a classifier is needed to classify each pixel as a vessel pixel or a non-vessel pixel such as k-nearest neighbors (KNN), feed-forward NN and Bayesian classifier.

All the supervised methods use a variety of approaches to calculate the feature vector and also to classify each pixel. Niemeijer et al. [19] introduce a long feature vector (31-Dimension) for each pixel consisting of the Gaussian filter and its derivatives at five scales. They also compare three classifiers and they show the performance of k-nearest neighbors (KNN) classifier is superior for all experiments. Staal et al. [20] also employed the same classifier, however they utilize ridge profiles to compute features for each pixel. On the other hand, some methods use a short feature vector. For instance, Soares et al. [21] utilize a six-D feature vector and Marin et al. [22] introduce a 7-D feature.

Although supervised methods are robust for many retinal images, they are costly in terms of processing time. They also need ground truth data that are already classified, which may not be available in real life applications. Therefore, supervised approaches are not as common as unsupervised algorithms for medical decision support systems and real time applications. As a result, we focused on unsupervised methods in this research. In this paper, we propose a new unsupervised algorithm based on a directional line sensitivity model of the human visual system to detect blood vessels in the retinal fundus images in almost real time.

3. The Proposed Method

Fundus images contain Red, Green, and Blue (RGB) images of the retina. The green channel and grey-level images provide the best vessel-background contrast of the RGB-representation, while the blue channel offers poor dynamic range and the red one is the brightest colour channel and has low contrast. Therefore, grey-level and green channel images are the best choices for image segmentation. In this research, we employed grey-level retinal images. A flow chart of our method is shown in Fig. 1 which consists of four main steps. These steps will be described in detail in the following sections.

3.1 Preprocessing

Retinal fundus images are not uniform images. The contrast of the retinal fundus images tends to be bright in the centre and diminish at the side, hence preprocessing is essential for minimizing this effect and to have a more uniform image. We introduce a simple technique to minimize the drift in image intensity and lack of image contrast, and generate a uniform image by using a median filter.

The principal function of median filters is to force points with distinct intensity to be more similar to their neighbors. Median filters are quite popular because they provide excellent noise-reduction (impulse noise) capabilities, with less blurring than linear smoothing filter of similar size. Median filters replace the value of a pixel by the median of the grey levels in the neighborhood of that pixel. Therefore, a median filter can be used to achieve the estimation of the background image and location of optic disc. The optic disc is a round area in the fundus images where retinal nerve fibers collect to form the optic nerve. To achieve this goal, the median filter must be large enough in size to remove blood vessels as a noise. The experimental results demonstrate that in 576×720 fundus images, employing a 25×25 median filter will remove blood vessels from the grey-level image and the background and optic disc will appear.

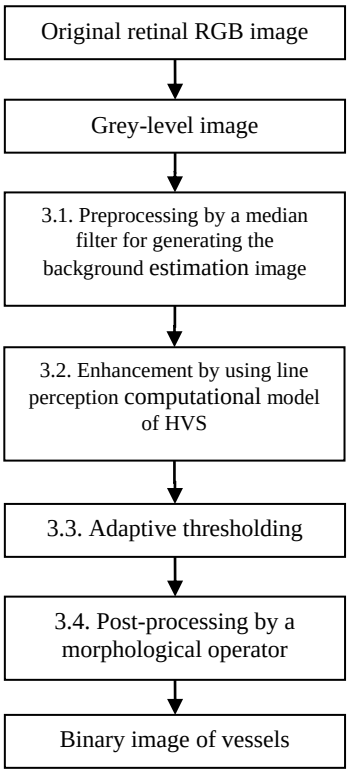

Fig. 1. A flow chart of the proposed method

If $i(x, y)$ is defined as a luminance distribution of original RGB input image and $g(x, y)$ is defined as a grey-level image of $i(x, y)$, then the background, *b(x, y)*, of a grey-level image is obtained by median filter with size of window 25×25. Fig. 2 (a) depicts an input original RGB image from a DRIVE database as (x, y), and Fig. 2 (b and c) illustrates the grey level of $i(x, y)$ and the output of median filter (i.e. $b(x, y)$), respectively. This clearly shows that the presented filter with the appropriate size is a good approximation of the background in retinal fundus images. Once the background is computed, a uniform

image is acquired by subtracting the background image from the grey-level image:

$$U(x,y) = g(x,y) - b(x,y) \quad (1)$$

This equation generates a uniform image. Fig. 2(d) shows the $U(x,y)$.

In order to enhance the blood vessel intensity, we need an image with vessel pixels containing brighter intensity than background pixels. This can be generated by using negative transformation:

$$s(x,y) = 255 - U(x,y) \quad (2)$$

Finally, to avoid processing the black border and corners, a binary mask is applied to $s(x,y)$. These two last steps are shown in Fig. 2 (e and f). Through the proposed preprocessing approach, a uniform and normalized image of the retina with vessel pixels brighter than non-vessel pixels is generated. In the next section, a novel vessel enhancement technique to increase vessel's intensity is presented.

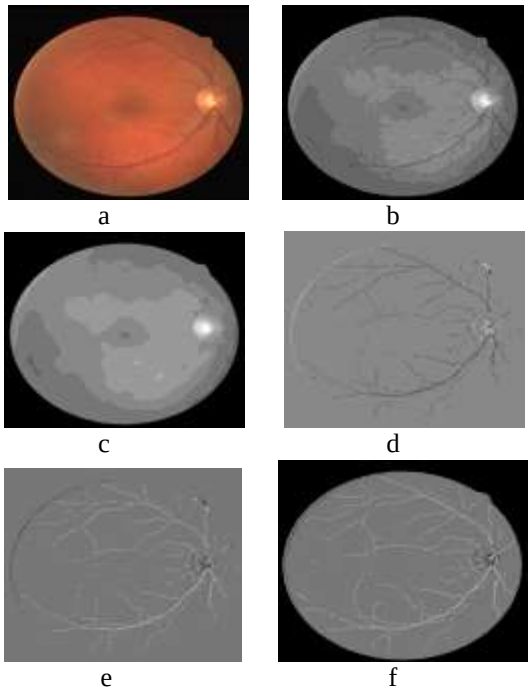

Fig. 2 Preprocessing steps (a) original RGB retinal image (b) grey-level image (c) result of the median filtering (d) result of subtracting background image from grey-level image (e) negative image (f) result of the preprocessing step.

3.2 Vessels Enhancement by Computational Model of a Simple Cell

Due to the poor local contrast of blood vessels, intensity of vessel pixels must be enhanced. The proposed method was motivated by neurons which respond to line and edge in the primary visual cortex. It is not feasible to build a computational model of HVS for image processing applications directly from the physiology of the HVS, due to its tremendous complexity. However, Computational models with different aspects of HVS were developed, aiming at observations from psychovisual experiments or sequential processing of the visual information in different layers of the HVS [22-27].

Hubel and Wiesel [28] identified two main classes of neuron which they called simple and complex cells. They proved that the majority of neurons in primary visual cortex reveal orientation selectivity [24-26]. Typically, such a neuron would react to a line or an edge of a given orientation in a given area of the visual field, called its receptive field (RF). Generally, simple cells are neurons which respond to an edge or growing/declining line, while neurons which do not react are called complex cells.

The computational models were extended based on simulation of the cell operation [23]. Simple cells are typically modeled by linear spatial summation followed by half-wave rectification. A family of two-dimensional Gabor functions was proposed as a model of the receptive field of simple cells [23,29]. A Gabor filter is a linear and local filter, and its kernel is multiplication of Gaussian and cosine functions. For an input image with luminance distribution of $s(x,y)$, a simple cell's response compute by convolution [27]:

$$S_{\sigma,\lambda,\theta_k,\varphi}(x,y) = h_{\sigma,\lambda,\theta_k,\varphi}(x,y) * s(x,y) \quad (3)$$

$$h_{\sigma,\lambda,\theta_k,\varphi}(x,y) = \cos\left(\frac{2\pi}{\lambda}\tilde{x} + \varphi\right) e^{-\frac{\tilde{x}^2+\gamma^2\tilde{y}^2}{2\sigma^2}} \quad (4)$$

$$\begin{bmatrix}\tilde{x}\\ \tilde{y}\end{bmatrix} = \begin{bmatrix}\cos\theta_k & \sin\theta_k\\ -\sin\theta_k & \cos\theta_k\end{bmatrix}\begin{bmatrix}x\\ y\end{bmatrix}$$

$$\theta_k = \frac{(k-1)\pi}{N_\theta} \quad \text{for} \quad k = 1,2,\dots,N_\theta \quad (5)$$

Where θ_k is the preferred orientation of a simple cell's response, $1/\lambda$ is spatial frequency, and N_θ is the number of total preferred orientations. Ellipticity of the receptive field and its symmetry with respect to the origin are controlled by constant parameter γ and angle parameter $\varphi \in (-\pi, \pi]$, respectively. The width of the receptive field of the simple cell is defined by a σ parameter. The ratio σ/λ determines the special frequency bandwidth, therefore it defines the number of parallel excitatory and inhibitory regions of the receptive field. In this research, we fix the ratio $\lambda = \sigma/0.56$ to have half-response bandwidth of one octave [27]. We also fix the parameter $\varphi = \pi$ to generate a symmetric $S_{\sigma,\lambda,\theta_k,\varphi}(x,y)$.In order to enhance vessel intensity, we employed the computational model of the simple cell (4) as a filter kernel to convolve with the preprocessed image. A block diagram of the proposed approach for improving blood vessels intensities based on the HVS line detection model is shown in Fig. 3.

The vessel enhancement process causes a side effect on non-vessel pixels which are similar to blood vessels. Non-vessel pixels are enhanced as much as blood vessels. These false vessel-like objects are related to some illnesses or various conditions in image acquisition. In order to suppress this side effect, a pruning function is proposed. This function is also motivated by operation of simple cells in the HVS. Simple cells in the HVS react to

an input signal when the output is greater than a particular threshold. Therefore, in each preferred orientation, we consider an adaptive threshold value on the cell responses, $S_{\sigma,\lambda,\theta_k,\varphi}(x,y)$. The pruning function is referred to as an activation function. We define the adaptive activation function $\mu_\alpha(x,y)$ as follows:

$$\mu_\alpha(x,y)=\begin{cases}1, & \text{if} \quad S_{\sigma,\lambda,\theta_k,\pi}(x,y)\geq \alpha\times\max(S_{\sigma,\lambda,\theta_k,\pi})\\ 0, & \text{if} \quad S_{\sigma,\lambda,\theta_k,\pi}(x,y)<\alpha\times\max(S_{\sigma,\lambda,\theta_k,\pi})\end{cases} \quad (6)$$

Constant parameter of $\alpha\ (0<\alpha\leq 1)$ controls the activation function. As a rule, there is a trade-off between salience of the thin vessels and signal to noise ratio. Although thin vessels are enhanced by setting high value for α, the false vessel-like objects are also highlighted.

The activation function $\mu_\alpha(x,y)$ must be applied to the cell response $S_{\sigma,\lambda,\theta_k,\pi}(x,y)$. As a result, the enhancement regions of $s(x,y)$ is computed by $E_{\sigma,,\theta_k,\alpha}(x,y)$ as follows:

$$E_{\sigma,\theta_k,\alpha}(x,y)=\mu_\alpha(x,y)\times S_{\sigma,\lambda,\theta_k,\pi}(x,y) \quad \text{for } \lambda={}^{\sigma}/_{0.56} \quad (7)$$

Experimental results demonstrated a significant role of the proposed adaptive activation function on Gabor filter responses. It improved the accuracy of the proposed method.

Finally, vessel enhancement is completed by combining the cell responses at various directions into a single output. After the kernel is rotated in N_θ directions, the maximum response is selected for each pixel. The output image is considered as a salient image.

$$SI_{\sigma,\alpha}(x,y)=\max\left(E_{\sigma,\theta_k,\alpha}(x,y)\right)$$

$$\text{for} \qquad k=1,2,\dots,N_\theta \quad (8)$$

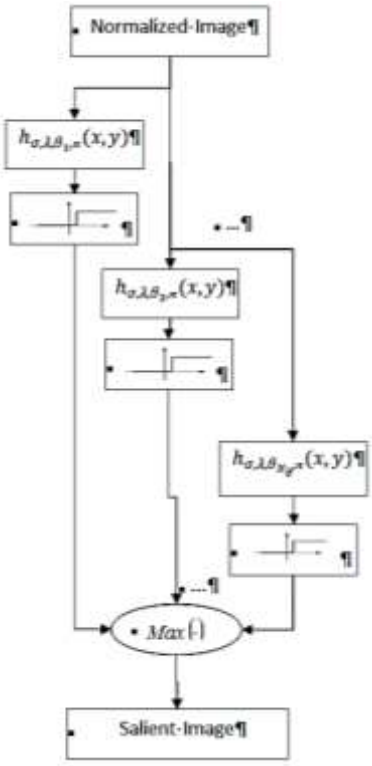

Fig. 3. A procedure of the proposed method for the blood vessels enhancement

3.3 Blood Vessels Segmentation

The output of our method must be a binary image with high value '1' for vessel pixels and low value '0' for non-vessel pixels. Due to the vessel enhancement step, the intensity of vessel pixels is considerably higher than non-vessel pixels, and they would be segmented by a simple threshold. Therefore, we generate the segmentation map by using a simple threshold. In other words, the adaptive threshold acts as a classifier and classifies each pixel as vessel or non-vessel to obtain the vessel binary image. The classifier is modified by intensity average as follows:

$$BM_{\sigma,\alpha,\beta}(x,y)=\begin{cases}1, & \text{if} \quad SI_{\sigma,\alpha}(x,y)\geq \beta\times\text{mean}(SI_{\sigma,\alpha})\\ 0, & \text{if} \quad SI_{\sigma,\alpha}(x,y)<\beta\times\text{mean}(SI_{\sigma,\alpha})\end{cases} \quad (9)$$

Where $BM_{\sigma,\alpha,\beta}(x,y)$ is the binary map of the blood vessels and β is a constant parameter which controls a ratio of vessel pixels and non-vessel pixels. We fixed β to 3/2 for the images.

3.4 Post-Processing

The last phase in our method is a local morphological process on the binary map to overcome the problems arising from over segmentation. Over-segmentation occurs because of lesions or noise in the original image. We can improve the output binary map by removing the lesion and noise areas. This can be done by a local morphological process. Generally, over-segmentation areas are smaller than the thinnest vessel. Hence, all connected objects which are smaller than the thinnest vessel should be removed. Practical experience demonstrated that the thinnest vessel has about 200 pixels in DRIVE [30] and STARE [31] databases. Consequently, in the binary maps, the objects whose areas are less than 200 pixels should be removed.

4. Experimental Results and Evaluation Metrics

4.1 Databases

We utilized the images included in the well-known DRIVE and STARE databases to assess the performance of the proposed method. The DRIVE database comprises 40 eye-fundus colour images. The image set is divided into a test and training sets and each one contains 20 retinal images. The test set is employed for measurement of performance of the vessel segmentation algorithms. The DRIVE database also provides two manual segmentations on each image of the test set which made by two different human observers. The manually segmented images by the 1st human observer are used as a gold-standard image (ground truth). In the STARE database, there is just one image set. It contains 20 images; ten of these contain pathology. It includes two manual segmentations by Hoover and Kouznetsova. The performance is computed with the segmentations of the 1st observer as a gold-standard image.

4.2 Metrics

Our algorithm is evaluated in terms of sensitivity *(Se)*, specificity *(Sp)*, positive predictive value *(Ppv)*, negative predictive value *(Npv)*, and accuracy *(Acc)*. *Se* and *Sp* metrics are the ratio of well-classified vessel and non-vessel pixels, respectively. *Ppv* and *Npv* are the ratio of pixels classified as vessel pixels and the ratio of pixels classified as background pixels which are both correctly classified. Finally, *Acc* is a global measurement, and provides the ratio of total well-classified pixels. These metrics are defined as:

$$\mathrm{Se} = \frac{\mathrm{TP}}{\mathrm{TP+FN}} \tag{10}$$

$$\mathrm{Sp} = \frac{\mathrm{TN}}{\mathrm{TN+FP}} \tag{11}$$

$$\mathrm{Ppv} = \frac{\mathrm{TP}}{\mathrm{TP+FP}} \tag{12}$$

$$\mathrm{Npv} = \frac{\mathrm{TN}}{\mathrm{TN+FN}} \tag{13}$$

$$\mathrm{Acc} = \frac{\mathrm{TP+TN}}{\mathrm{TP+FN+TN+FP}} \tag{14}$$

Where *TP* is the number of pixels correctly classified as vessel pixels; *TN* is the number of pixels correctly classified as non-vessel pixels; *FN* is the pixels belonging to a vessel, but is recognized as background pixels. *FP* is the pixels incorrectly classified as vessel pixels.

The proposal method was implemented on a Windows-7 operating system running on an Intel Pentium 2.7 GHz processor with 4 G RAM. In the implementation of the proposal method, N_θ is set at 8, or the angle resolution is 22.5◦ which is able to be aligned with vessels in different directions. The constant value of α is fixed at 0.16 for DRIVE database and 0.14 for STARE database. The width of the receptive field of simple cells (σ parameter) is set at 0.6 and the ellipticity of the receptive field (γ parameter) is set at 0.4. They found by iteration to match the filter properly with vessels. As all parameters in Gabor filter are constant, there is no need for ROC curve. The required mask images for the preprocessing step are available in the DRIVE database. For the STARE database, we have generated the mask images as the STARE database did not provide them.

4.3 Results

The performance results of the DRIVE and STARE databases are shown in Table 1 and Table 2. The last rows of the tables show average *Se*, *Sp*, *Ppv*, *Npv*, and *Acc* values in each database. The maximum and minimum values are in bold. It can be perceived that the average sensitivity value on DRIVE images is higher than STARE images from the tables. The minimum values of *Se* are also 0.6650 and 0.4858 on the DRIVE and STARE databases respectively, i.e. our method is more appropriate for the DRIVE than the STARE regarding the ratio of well-classified vessel pixels.

In terms of accuracy, the average values are 0.9403 and 0.9445 for the DRIVE and STARE databases, respectively. The accuracy of the proposed method on both databases is almost the same. Although the minimum accuracy of the STARE database (0.9150) is a weakness of our method, the average accuracy values are comparable with other results in the literature for both databases.

Two examples of the proposed segmentations from both databases along with gold standard segmentations are given in Fig. 4 and 5. In terms of quality, the proposed method is comparable with the related gold standards.

Table 1. Performance results on DRIVE database images

image	Se	Sp	Ppv	Npv	Acc
1	0.8090	0.9533	0.6889	0.9750	0.9369
2	0.7734	0.9718	0.7967	0.9677	0.9470
3	0.7319	0.9671	0.7579	0.9624	0.9380
4	0.7408	0.9672	0.7456	0.9664	0.9412
5	0.6993	0.9768	**0.8015**	0.9604	0.9440
6	0.6723	0.9757	0.7942	0.9552	0.9385
7	0.6929	0.9697	0.7471	0.9607	0.9380
8	0.7512	0.9444	0.6223	0.9689	0.9234
9	0.6486	**0.9802**	0.7919	0.9600	0.9456
10	0.7108	0.9706	0.7419	0.9658	0.9430
11	0.6921	0.9674	0.7357	0.9599	0.9355
12	0.7412	0.9661	0.7263	0.9685	0.9417
13	0.6650	0.9734	0.7785	0.9538	0.9354
14	0.7879	0.9566	0.6741	0.9754	0.9394
15	0.8141	0.9470	0.6077	0.9806	0.9349
16	0.7250	0.9730	0.7719	0.9657	0.9453
17	0.7137	0.9678	0.7220	0.9665	0.9412
18	0.7579	0.9688	0.7270	0.9733	0.9480
19	0.8185	0.9559	0.6856	0.9782	0.9414
20	**0.8219**	0.9610	0.6823	**0.9814**	**0.9481**
Average	**0.7384**	**0.9657**	**0.7300**	**0.9673**	**0.9403**

Table 2. Performance results on STARE database images

image	Se	Sp	Ppv	Npv	Acc
1	0.7309	0.9391	0.5587	0.9707	0.9192
2	0.6792	0.9448	0.5216	0.9708	0.9232
3	0.7574	0.9542	0.5649	0.9804	0.9399
4	0.5176	0.9795	0.7039	0.9556	0.9396
5	0.681	0.9704	0.7314	0.9626	0.9398
6	0.8404	0.9493	0.6030	0.9848	0.9401
7	0.8485	0.9641	0.7185	0.9833	0.9528
8	**0.8620**	0.9625	0.6971	**0.9858**	0.9533
9	0.8059	0.9685	0.7335	0.9789	0.9528
10	0.7907	0.9286	0.5479	0.9759	0.9150
11	0.7827	0.9747	0.7605	0.9776	0.9568
12	0.8312	0.9779	0.7976	0.9823	0.9640
13	0.7841	0.9660	0.7340	0.9739	0.9465
14	0.7945	0.9627	0.7201	0.9749	0.9446
15	0.7280	0.9720	0.7522	0.9683	0.9465
16	0.7714	0.9426	0.6413	0.9687	0.9224
17	0.7935	0.9619	0.7219	0.9739	0.9433
18	0.4858	**0.9964**	**0.8985**	0.9674	0.9652
19	0.5595	0.9907	0.7712	0.9758	**0.9679**
20	0.6319	0.9846	0.7756	0.9696	0.9573
Average	**0.7338**	**0.9645**	**0.6977**	**0.9741**	**0.9445**

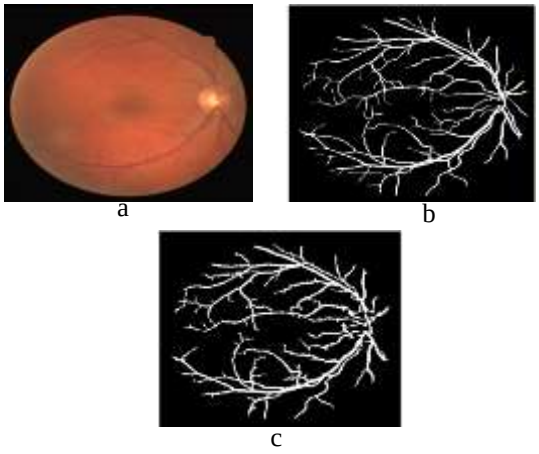

Fig. 4. Sample result of the proposed algorithm (a) the image number 20 from DRIVE database (b) the gold standard (c) result of the binary image of the proposed method

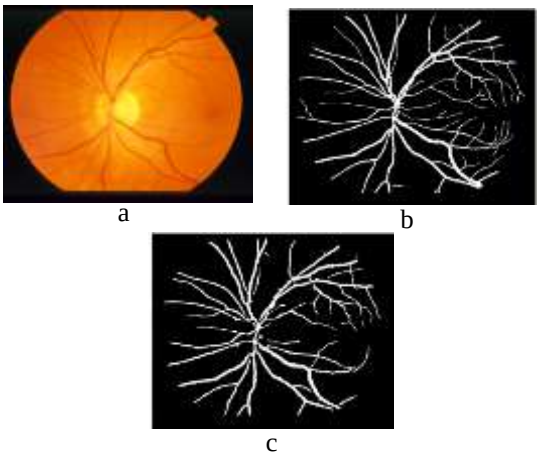

Fig. 5. Sample result of the proposed algorithm (a) the image number 12 from STARE database (b) the gold standard (c) result of the binary image of the proposed method.

4.4 Evaluation

In order to evaluate the performance of the proposed method, we compare our simulation results with the state-of- the-art results and hand-labeled ground truth segmentations in Table 3. The performance of the proposed method is evaluated based on two criteria: the value of accuracy (*Acc*) to measure the ability of hard-classification, and the 'sensitivity' (*Se*) to measure the ratio of well-classified vessel pixels. The results of Zana [11] and Jiang [32] were taken from the DRIVE database website [30]. A comparative analysis shows that the proposed method achieved better performance metrics than most of the unsupervised methods.

In general, supervised methods outperform unsupervised methods. However, even though our method is unsupervised, sensitivity values of the proposed method for STARE and DRIVE databases are almost higher than the supervised methods. Although Fraz et al [6], Al-Diri et al. [16] and You [33] seem to present better results than our approach, they suffer from high computational complexity and execution time when finding the vessels.

The performance of our method in terms of accuracy is almost superior when compared to unsupervised approaches. Clearly, sensitivity values of unsupervised methods are inferior or not accessible; however, a few methods provide higher accuracy than the proposed approach. In Lam et al. method [15], which presented the highest accuracy among all other methods, the sensitivities were not reported and more importantly it takes 13 minutes to generate the binary image. Table 4 shows the elapsed time comparison among our method with some state-of-the-art algorithms. A comparative analysis shows that Amin et al. [10] method has presented the fastest algorithm among the state-of-the-art algorithms with 0.9081 and 0.9191 accuracy values on STARE and DRIVE databases, respectively. The proposed method is implemented on 2.7GHz machine, which is ((2.7-2.66)/2.66) ×100 = 1.5% increase in machine speed compared to the machine (2.66 GHz) that Amin et al. used. As a result, their method which took 10 seconds on 2.66 GHz machine, will take $10/(1+0.015) \approx 9.85$ seconds on a 2.7 GHz machine. Therefore, the proposed method improves the execution time by about 50% and also presents more accuracy. Consequently, in terms of algorithm speed, the proposed method outperforms all other blood vessel segmentation methods.

5. Conclusion

Automatic segmentation of the retinal blood vessel is the first step in developing a computer-assisted diagnostic system. Extracting blood vessel in the fundus image is a challenging problem. We presented an effective and fast retinal vessel segmentation technique based on the simple cell operation of a primary visual cortex by using a Gabor filter. The proposed method is a fast and simple unsupervised method which does not require any training. The performance of this method was shown by sensitivity, specificity, positive predictive value, negative predictive value and accuracy measurements on DRIVE and STARE databases. Our method consists of four steps: preprocessing, blood vessel enhancement, adaptive thresholding, and post-processing.

Preprocessing is a mandatory step for almost all medical images because of the signal noise, drift in image intensity, and lack of the image contrast. First, we utilized a median filter for preprocessing to generate a uniform image from fundus images. Although, we are not pioneers in using a median filter, we utilized the median filter for fundus images to generate a uniform image. Then, blood vessel enhancement was accomplished based on the simple cell operation in the primary visual cortex. We utilized a directional Gabor filter at eight directions to increase blood vessel intensity. All parameters for the Gabor filter were fixed and did not require to be changed for each image. Next, adaptive thresholding was used to generate a binary image. Adaptive thresholding was utilized as a simple classifier to classify each pixel as a vessel pixel or non-vessel pixel. Finally, a local morphological process was used on the binary image to overcome the problems arising from lesions or noise.

There are solely two variable parameters, α and β, in our method to compromise the accuracy and the sensitivity. Although α and β were fixed in our implementation, they can be changed according to the requirements of its application.

The proposed method outperforms almost all other unsupervised state-of-the-art methods in terms of accuracy, sensitivity and speed. The proposed method is able to acquire the blood vessels in retinal images at about five seconds with an average accuracy of 0.9445 and 0.9403 for the STARE and DRIVE databases, respectively. However, due to a trade-off between the detection of narrow vessels and noise in our approach, several spots are falsely segmented as vessels.

We aim to improve the proposed method by applying a multi-scale Gabor filter instead of a single-scale filter in the future work. The proposed method may be also modified by applying some standard classifiers like the K-Nearest Neighbors algorithm instead of adaptive thresholding to increase the accuracy.

Table 3. Performance results compared to other methods on the STARE and DRIVE databases

Segmentation Methods	**Year**	**STARE database**		**DRIVE database**		**Method type**
		se	**Acc**	**Se**	**Acc**	
2nd human observer		0.8951	0.9348	0.7796	0.9470	**Hand labeled**
Niemeijer [19]	2004	N.A	N.A	N.A	0.9416	**Supervised Methods**
Soares [21]	2006	0.7207	0.9480	0.7332	0.9466	
Staal [20]	2004	N.A	0.9516	N.A	0.9441	
Marin [22]	2011	0.6944	0.9526	0.7067	0.9452	
Fraz [6]	2012	0.7548	0.9534	0.7406	0.9480	
Hoover [7]	2000	0.6747	0.9264	N.A	N.A	**Unsupervised Methods**
Zana [11]	2001	N.A	N.A	0.6971	0.9377	
Jiang [32]	2003	N.A	0.9009	N.A	0.9212	
Mendonca [13]	2006	0.6996	0.9440	0.7344	0.9452	
Lam [14]	2008	N.A	0.9474	N.A	N.A	
Al-Diri [16]	2009	0.7521	N.A	0.7282	N.A	
Cinsdikici [9]	2009	N.A	N.A	N.A	0.9293	
Lam [15]	2010	N.A	0.9567	N.A	0.9472	
Fraz [12]	2011	0.7311	0.9442	0.7152	0.9430	
You [33]	2011	0.7260	0.9497	0.7410	0.9434	
Amin [10]	2011	0.7261	0.9081	0.6608	0.9191	
Proposed Method	**2014**	**0.7338**	**0.9445**	**0.7384**	**0.9403**	

N.A: Not Available

Table 4. Comparison of the execution times based on STARE and DRIVE databases

Vessel detection method	**Computer configuration**	**STARE**	**DRIVE**	**Execution time**
		Acc	**Acc**	
Manual segmentation	Second observer	0.9348	0.9470	120 min
Lam [14]	MATLAB, Intel Pentium 2.66 GHz, 512 MB RAM	0.9474	N.A	25 min
Lam [15]	MATLAB, Duo CPU 1.83 GHz, 2 GB RAM	0.9567	0.9472	13 min
Soares [21]	MATLAB, AMD Athlon 2.2 GHz, 1 G RAM	0.9480	0.9466	3 min 10 s
Staal [20]	N.A, Intel Pentium 1 GHz, 1 G RAM	0.9516	0.9441	15 min
Al-Diri [16]	MATLAB, 1.2 GHz Pentium system	N.A	N.A	11 min
Amin [10]	MATLAB, Intel Pentium 2.66 GHz, 512 MB RAM	0.9081	0.9191	10 s
Cinsdikici [9]	N.A		0.9293	35 s
The Proposed Method	**Intel Pentium 2.7 GHz, 4 G RAM**	**0.9445**	**0.9403**	**5 s**

N.A: Not Available

References

[1] B. Bowling, Kanski's Clinical Ophthalmology: A Systematic Approach, Eighth ed. Sydney, Australia: Elsevier Health Science, 2015.

[2] M. Esmaeili, H. Rabbani, A. Dehnavi, and A. Dehghani, "Automatic detection of exudates and optic disk in retinal images using curvelet transform," IET image processing, vol. 6, pp. 1005-1013, 2012.

[3] S. W. Franklin and S. E. Rajan, "Diagnosis of diabetic retinopathy by employing image processing technique to detect exudates in retinal images," IET Image Processing, vol. 8, pp. 1-9, 2014.

[4] M. J. Fowler, "Microvascular and macrovascular complications of diabetes," Clinical Diabetes, vol. 26, pp. 77-82, 2008.

[5] J. Anitha, C. K. S. Vijila, and D. J. Hemanth, "An Overview of Computational Intelligence Techniques for Retinal Disease Identification Applications," International Journal of Reviews in Computing, vol. 5, pp. 29-46, 2009.

[6] M. M. Fraz, P. Remagnino, A. Hoppe, B. Uyyanonvara, A. R. Rudnicka, C. G. Owen, et al., "An ensemble classification-based approach applied to retinal blood vessel segmentation," Biomedical Engineering, IEEE Transactions on, vol. 59, pp. 2538-2548, 2012.

[7] A. Hoover, V. Kouznetsova, and M. Goldbaum, "Locating blood vessels in retinal images by piecewise threshold probing of a matched filter response," Medical Imaging, IEEE Transactions on, vol. 19, pp. 203-210, 2000.

[8] L. Gang, O. Chutatape, and S. M. Krishnan, "Detection and measurement of retinal vessels in fundus images using amplitude modified second-order Gaussian filter," Biomedical Engineering, IEEE Transactions on, vol. 49, pp. 168-172, 2002.

[9] M. G. Cinsdikici and D. Aydın, "Detection of blood vessels in ophthalmoscope images using MF/ant (matched filter/ant colony) algorithm," Computer methods and programs in biomedicine, vol. 96, pp. 85-95, 2009.

[10] M. A. Amin and H. Yan, "High speed detection of retinal blood vessels in fundus image using phase congruency," Soft Computing, vol. 15, pp. 1217-1230, 2011.
[11] F. Zana and J.-C. Klein, "Segmentation of vessel-like patterns using mathematical morphology and curvature evaluation," Image Processing, IEEE Transactions on, vol. 10, pp. 1010-1019, 2001.
[12] M. Fraz, S. Barman, P. Remagnino, A. Hoppe, A. Basit, B. Uyyanonvara, et al., "An approach to localize the retinal blood vessels using bit planes and centerline detection," Computer methods and programs in biomedicine, 2011.
[13] A. M. Mendonca and A. Campilho, "Segmentation of retinal blood vessels by combining the detection of centerlines and morphological reconstruction," Medical Imaging, IEEE Transactions on, vol. 25, pp. 1200-1213, 2006.
[14] B. S. Lam and H. Yan, "A novel vessel segmentation algorithm for pathological retina images based on the divergence of vector fields," Medical Imaging, IEEE Transactions on, vol. 27, pp. 237-246, 2008.
[15] B. S. Lam, Y. Gao, and A.-C. Liew, "General retinal vessel segmentation using regularization-based multiconcavity modeling," Medical Imaging, IEEE Transactions on, vol. 29, pp. 1369-1381, 2010.
[16] B. Al-Diri, A. Hunter, and D. Steel, "An active contour model for segmenting and measuring retinal vessels," Medical Imaging, IEEE Transactions on, vol. 28, pp. 1488-1497, 2009.
[17] G. Gardner, D. Keating, T. Williamson, and A. Elliott, "Automatic detection of diabetic retinopathy using an artificial neural network: a screening tool," British journal of Ophthalmology, vol. 80, pp. 940-944, 1996.
[18] C. Sinthanayothin, J. F. Boyce, H. L. Cook, and T. H. Williamson, "Automated localisation of the optic disc, fovea, and retinal blood vessels from digital colour fundus images," British Journal of Ophthalmology, vol. 83, pp. 902-910, 1999.
[19] M. Niemeijer, J. Staal, B. van Ginneken, M. Loog, and M. D. Abramoff, "Comparative study of retinal vessel segmentation methods on a new publicly available database," in Medical Imaging 2004, pp. 648-656.
[20] J. Staal, M. D. Abràmoff, M. Niemeijer, M. A. Viergever, and B. van Ginneken, "Ridge-based vessel segmentation in color images of the retina," Medical Imaging, IEEE Transactions on, vol. 23, pp. 501-509, 2004.
[21] J. V. Soares, J. J. Leandro, R. M. Cesar, H. F. Jelinek, and M. J. Cree, "Retinal vessel segmentation using the 2-D Gabor wavelet and supervised classification," Medical Imaging, IEEE Transactions on, vol. 25, pp. 1214-1222, 2006.
[22] D. Marín, A. Aquino, M. E. Gegúndez-Arias, and J. M. Bravo, "A new supervised method for blood vessel segmentation in retinal images by using gray-level and moment invariants-based features," Medical Imaging, IEEE Transactions on, vol. 30, pp. 146-158, 2011.
[23] J. P. Jones and L. A. Palmer, "An evaluation of the two-dimensional Gabor filter model of simple receptive fields in cat striate cortex," Journal of Neurophysiology, vol. 58, pp. 1233-1258, 1987.
[24] D. G. Albrecht and W. S. Geisler, "Motion selectivity and the contrast-response function of simple cells in the visual cortex," Visual neuroscience, vol. 7, pp. 531-546, 1991.
[25] D. C. Somers, S. B. Nelson, and M. Sur, "An emergent model of orientation selectivity in cat visual cortical simple cells," The Journal of neuroscience, vol. 15, pp. 5448-5465, 1995.
[26] D. Ferster, S. Chung, and H. Wheat, "Orientation selectivity of thalamic input to simple cells of cat visual cortex," Nature, vol. 380, pp. 249-252, 1996.
[27] C. Grigorescu, N. Petkov, and M. A. Westenberg, "Contour detection based on nonclassical receptive field inhibition," Image Processing, IEEE Transactions on, vol. 12, pp. 729-739, 2003.
[28] D. H. Hubel and T. N. Wiesel, "Receptive fields, binocular interaction and functional architecture in the cat's visual cortex," The Journal of physiology, vol. 160, p. 106, 1962.
[29] J. G. Daugman, "Uncertainty relation for resolution in space, spatial frequency, and orientation optimized by two-dimensional visual cortical filters," Optical Society of America, Journal, A: Optics and Image Science, vol. 2, pp. 1160-1169, 1985.
[30] Research Section, Digital Retinal Image for Vessel Extraction(DRIVE) Database. Utrecht, The Netherlands, Univ. Med. Center Utrecht, Image Sci. Inst. [Online]. Available: http://www.isi.uu.nl/Research/Databases/DRIVE/ [Feb. 1, 2016]
[31] STARE database, STARE ProjectWebsite. Clemson, SC, Clemson Univ. [Online]. Available: http://www.ces.clemson.edu/~ahoover/stare/ [Feb. 1, 2016]
[32] X. Jiang and D. Mojon, "Adaptive local thresholding by verification-based multithreshold probing with application to vessel detection in retinal images," Pattern Analysis and Machine Intelligence, IEEE Transactions on, vol. 25, pp. 131-137, 2003.
[33] X. You, Q. Peng, Y. Yuan, Y.-m. Cheung, and J. Lei, "Segmentation of retinal blood vessels using the radial projection and semi-supervised approach," Pattern Recognition, vol. 44, pp. 2314-2324, 2011.

Mohsen Zardadi received his M.Sc degree in 2006 from Ferdowsi University of Mashhad, Mashhad, Iran in Electrical Engineering. Since 2012 he has been pursuing his Ph.D degree in the Department of Electrical and Computer Engineering of Birjand University, Birjand, Iran. His research interests include computer vision and image processing.

Nasser Mehrshad received the B.Sc degree from Ferdowsi University of Mashhad, Mashhad, Iran, in 1995 and the M.Sc and Ph.D degrees from Tarbiat Modares University, Tehran, Iran, in 1998 and 2005, respectively, both in Biomedical Engineering. He is currently an Associate Professor in the Department of Electrical and Computer Engineering, the University of Birjand, Birjand, Iran. His research interests include Computer Vision, Digital Signal and Image Processing, Biometrics and Biomedical Data Mining.

Seyyed Mohammad Razavi received the B.Sc degree in Electrical Engineering from Amirkabir University of Technology, Tehran, Iran, in 1994 and the M.Sc degree in Electrical Engineering from the Tarbiat Modares University, Tehran, Iran, in 1996, and the Ph.D degree in Electrical Engineering from the Tarbiat Modares University, Tehran, Iran, in 2006. Now, he is an Associate Professor in the Department of Electrical and Computer Engineering, the University of Birjand, Birjand, Iran. His research interests include Computer Vision, Pattern Recognition and Artificial Intelligence Algorithms.